



HAL
open science

Sharp transition to strongly anomalous transport in unsaturated porous media

Andrés Velásquez-parra, Tomás Aquino, Matthias Willmann, Yves Méheust,
Tanguy Le Borgne, Joaquín Jiménez-martínez

► **To cite this version:**

Andrés Velásquez-parra, Tomás Aquino, Matthias Willmann, Yves Méheust, Tanguy Le Borgne, et al..
Sharp transition to strongly anomalous transport in unsaturated porous media. *Geophysical Research
Letters*, 2022, 49 (3), pp.e2021GL096280. 10.1029/2021GL096280 . insu-03537085v2

HAL Id: insu-03537085

<https://insu.hal.science/insu-03537085v2>

Submitted on 24 Feb 2022

HAL is a multi-disciplinary open access archive for the deposit and dissemination of scientific research documents, whether they are published or not. The documents may come from teaching and research institutions in France or abroad, or from public or private research centers.

L'archive ouverte pluridisciplinaire **HAL**, est destinée au dépôt et à la diffusion de documents scientifiques de niveau recherche, publiés ou non, émanant des établissements d'enseignement et de recherche français ou étrangers, des laboratoires publics ou privés.



Distributed under a Creative Commons Attribution - NonCommercial - NoDerivatives 4.0
International License

Geophysical Research Letters[®]



RESEARCH LETTER

10.1029/2021GL096280

Key Points:

- The presence of an immiscible phase in porous media leads to an abrupt shift in the scaling of the liquid-phase velocity distribution
- Dispersion is quasi-Fickian in saturated systems but becomes quasi-ballistic under even slightly unsaturated conditions
- We predict flow and advective transport based on phase distribution and porous medium geometry

Supporting Information:

Supporting Information may be found in the online version of this article.

Correspondence to:

J. Jiménez-Martínez,
joaquin.jimenez@eawag.ch;
jjimenez@ethz.ch

Citation:

Velásquez-Parra, A., Aquino, T., Willmann, M., Méheust, Y., Le Borgne, T., & Jiménez-Martínez, J. (2022). Sharp transition to strongly anomalous transport in unsaturated porous media. *Geophysical Research Letters*, 49, e2021GL096280. <https://doi.org/10.1029/2021GL096280>

Received 21 SEP 2021

Accepted 21 DEC 2021

Sharp Transition to Strongly Anomalous Transport in Unsaturated Porous Media

Andrés Velásquez-Parra^{1,2} , Tomás Aquino³ , Matthias Willmann² , Yves Méheust³ , Tanguy Le Borgne³ , and Joaquín Jiménez-Martínez^{1,2} 

¹Department of Water Resources and Drinking Water, Swiss Federal Institute of Aquatic Science and Technology, Eawag, Dübendorf, Switzerland, ²Department of Civil, Environmental and Geomatic Engineering, ETH Zürich, Zürich, Switzerland, ³University Rennes, CNRS, Géosciences Rennes, UMR, Rennes, France

Abstract The simultaneous presence of liquid and gas in porous media increases flow heterogeneity compared to saturated flows. However, the impact of saturation on flow and transport has so far remained unclear. The presence of gas in the pore space leads to flow reorganization. We develop a theoretical framework that captures the impact of that reorganization on pore-scale fluid velocities. Preferential flow is distributed spatially through a backbone, and flow recirculation occurs in flow dead-ends. We observe, and predict theoretically, that this previously identified flow structure induces a marked change in the scaling of the velocity probability density function compared to the saturated configuration and a sharp transition to strongly anomalous transport. We develop a transport model using the continuous time random walk theory that predicts advective transport dynamics for all saturation degrees. Our results provide a new modeling framework linking phase heterogeneity to flow heterogeneity in unsaturated porous media.

Plain Language Summary The unsaturated zone, where water and air coexist in the pore space, extends between the soil surface and the groundwater level. Its pronounced structural heterogeneity induces complex flow patterns, which lead to rich solute transport behaviors. Inputs (precipitation) and outputs (evaporation and deep drainage) induce spatiotemporal variability in water saturation (i.e., fraction of the pore space occupied by water), which impacts flow, transport, and biochemical reactions. It has been observed that water-unsaturated conditions lead to a strong separation of flow in regions of high velocity, where most of the fluid is transported, and regions of low velocity. We identify the spatial distribution and size of the low-velocity regions as key control features on water flow and transport of dissolved chemical species, leading to transport behaviors that differ from those described by classical transport formulations. We use these findings to develop a theoretical framework that allows us to predict flow and advective transport under unsaturated conditions, based on parameters that describe the heterogeneity in phase distribution within the pore space and that are directly linked to the geometry of the system. These results represent a decisive step toward the prediction of fate and transport phenomena from structural properties in unsaturated porous media.

1. Introduction

Unsaturated porous media, where liquid and gas phases coexist, play a central role in a broad range of environmental and industrial applications, including contaminant transport (Lahav et al., 2010; Sebilo et al., 2013), artificial groundwater recharge (Bouwer, 2002), underground gas storage (Panfilov, 2010), radioactive waste disposal (Winograd, 1981), and energy storage (Barbier, 2002), among others. Previous studies have shown that under saturated conditions, that is, for single-phase flow, structural heterogeneity in the solid phase is sufficient to induce anomalous transport (de Anna et al., 2013; Holzner et al., 2015; Kang et al., 2014; Le Borgne et al., 2011; Morales et al., 2017; Moroni et al., 2007; Stoop et al., 2019). This typically translates to early solute arrival and longer tailing at a given control plane, as well as non-Fickian scaling of spatial solute spreading (Berkowitz et al., 2006; Bijeljic et al., 2011), all features that cannot be described using classical transport formulations.

In unsaturated porous media, the presence of several immiscible or partially miscible fluid phases in the pore space induces complex flow topologies, increasing flow tortuosity, and resulting in more extreme high and low velocities (Birkholzer & Tsang, 1997; Datta et al., 2013; de Gennes, 1983; Jiménez-Martínez et al., 2017; Nützmann et al., 2002; Wildenschild & Jensen, 1999). The consequences of this heterogeneity for solute transport properties remain controversial. Both an increase (Aziz et al., 2018; Bromly & Hinz, 2004; Haga et al., 1999;

© 2022. The Authors.

This is an open access article under the terms of the [Creative Commons Attribution-NonCommercial-NoDerivs License](https://creativecommons.org/licenses/by-nc-nd/4.0/), which permits use and distribution in any medium, provided the original work is properly cited, the use is non-commercial and no modifications or adaptations are made.

Padilla et al., 1999) and a decrease (Birkholzer & Tsang, 1997; Vanderborght & Vereecken, 2007) of dispersion with decreasing saturation have been reported. However, these studies have resorted to continuum/effective-scale theories, where the use of locally averaged velocity values does not reflect the complexity of the pore-scale velocity field.

Here, we use images from millifluidic experiments and pore-scale numerical simulations to derive a new theoretical framework linking medium structure parameters and saturation degree (S_w , fraction of the pore volume occupied by the liquid) to the probability density function (PDF) of both flow rate through pore throats and velocities and to anomalous transport dynamics. We identify a previously unknown abrupt change in the velocity statistics, which become much broader even for low desaturations. Our theory is built on the partition of the pore space into two contrasting structures, a backbone of preferential flow paths and dead-end regions of low velocity. While the backbone/dead-end structure is known since the work of de Gennes (1983), dead-ends were simply assumed to have zero velocities, and its direct impact on velocity statistics remained unknown. Our theory elucidates the mechanisms leading to the observed transition and predicts the change exerted by the presence of dead-ends on the velocity PDF scaling for unsaturated systems, compared to fully saturated conditions. Using a continuous time random walk (CTRW) approach, parameterized according to the theoretical velocity PDFs, we predict a transition from quasi-Fickian to highly anomalous, quasi-ballistic transport in unsaturated systems, in agreement with resolved simulations.

2. Methods

2.1. Numerical Flow Simulations

We employ experimental images of a quasi two-dimensional (2D) porous medium characterizing the arrangement of two immiscible phases (water and air) under different S_w (1.00, 0.83, 0.77, and 0.71; Jiménez-Martínez et al., 2017) and simulate flow at the pore scale. Experiments were performed for low capillary numbers, hence the air clusters (nonwetting phase) remain immobile (Tang et al., 2019). Under these conditions, variations in the viscosity of the nonwetting phase are not relevant. The dimensions of the system are 132 mm \times 87 mm, and its thickness (vertical gap) $h = 0.5$ mm. The average pore-throat width (shortest distance between grains) $a_m = 1.17$ mm, and the mean pore size (meeting point of pore throats) $\lambda = 1.85$ mm, leading to a porosity of 0.71, similar to that reported in other studies addressing 2D systems (Andrade et al., 1997; Tallakstad et al., 2009).

We numerically simulate 2D steady-state Stokes flow, in which the flow of water around the solid grains and air bubbles is exclusively controlled by viscous dissipation. The effect of the third dimension on depth-averaged flow is introduced in the Stokes equation through a Darcy-like term (Ferrari et al., 2015) representing the drag force exerted on the liquid by the upper and lower walls in the experimental configuration (Jiménez-Martínez et al., 2017). A constant flow rate of 1.375 mm³/s for the saturated case and 0.277 mm³/s for the unsaturated cases is imposed at the inlet (Jiménez-Martínez et al., 2017). Atmospheric pressure is imposed at the outlet. We assign a no-slip boundary condition to solid–liquid interfaces and a slip boundary condition to liquid–gas interfaces, that is, zero longitudinal stress is imposed along these interfaces rather than a zero velocity (Kazemifar et al., 2016).

2.2. Particle Tracking Simulations

To investigate the consequences of our velocity analysis for advective transport, we also perform advective particle tracking simulations to allow for a numerical quantification of dispersion. We perform a flux-weighted injection of 10^4 particles along the inlet boundary of the porous medium, over an area with a length equal to the medium width in the y -direction and a width equal to the average grain size (i.e., 0.83 mm) along the x -axis. Particle positions are tracked isochronically over fixed time steps Δt (t -Lagrangian sampling). For $S_w = 1.00$, $\Delta t = 0.05 t_a$, where $t_a = \lambda/\bar{v}$ is the advective time over the mean pore size λ at the mean velocity \bar{v} . For the unsaturated cases, Δt ranges between $0.021 t_a$ and $0.029 t_a$. A 100 times finer time discretization is introduced at early times to improve resolution in the ballistic dispersion regime.

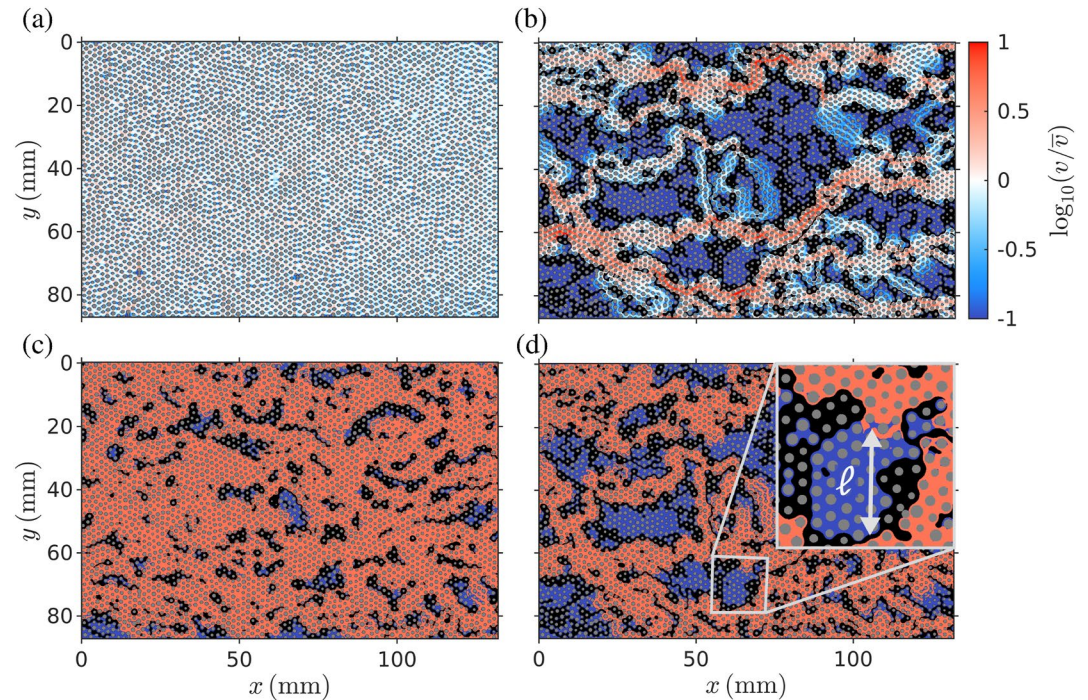


Figure 1. Velocity fields obtained from Stokes flow numerical simulations, displayed in terms of the velocity magnitude v normalized by its mean value \bar{v} , for (a) $S_w = 1.00$ and (b) $S_w = 0.71$. The colorbar is common to (a) and (b), with red colors indicating high velocities and blue colors low velocities. Regions where $\log_{10}(v/\bar{v}) \leq -1$ are shown in the darkest blue tone. The solid phase (circular obstacles) is shown in gray and air clusters in black. (c, d) show the partition of the velocity field into two types of flow structures: (i) backbone or preferential paths, depicted in red, and (ii) dead-end regions of low velocity, depicted in blue, for $S_w = 0.83$ and $S_w = 0.71$, respectively. The inset in (d) depicts the geometry of a dead-end region, with ℓ representing the dead-end region's depth.

3. Prediction of Unsaturated Flow Distribution

3.1. Impact of Saturation on Flow Velocities

While the simulated velocity fields exhibit limited variability under saturated conditions (Figure 1a), the flow heterogeneity is strongly enhanced in the unsaturated case (Figure 1b). The introduction of air induces a partition of the flow field into two flow structures (de Gennes, 1983): a backbone of preferential flow paths and dead-end regions (velocity is nonzero [Jiménez-Martínez et al., 2015, 2017]) that branch out from the backbone (Figures 1c and 1d). For the Eulerian velocity PDF $p_E(v)$, this reorganization of flow compared to the saturated case leads to an increase in the probability of low velocities (Figure 2a), as they are encountered not only close to the solid–liquid interfaces but also within dead-end regions (Figure 1b). This is described by the sharp transition from a plateau for $S_w = 1.00$ to a power-law-like behavior for $S_w < 1.00$. High velocities follow an exponential trend, in agreement with existing literature (Datta et al., 2013), and can be characterized by a saturation-dependent characteristic velocity v_c .

We partition the flow field into backbone and dead-end regions (Figures 1c and 1d) by selecting a velocity threshold at the transition between the power law and exponential velocity regimes. Results suggest a more accentuated flow separation with lower saturation, where dead-end regions increase in both size and number as S_w decreases, and where the dead-end area PDF p_A decays as a power law (Figure 3). Note that previous studies in 2D porous media have analyzed air cluster area distributions, rather than fluid dead-end area distributions, and found a power law behavior with an exponential cutoff at large cluster sizes (Jiménez-Martínez et al., 2017; Tallakstad et al., 2009).

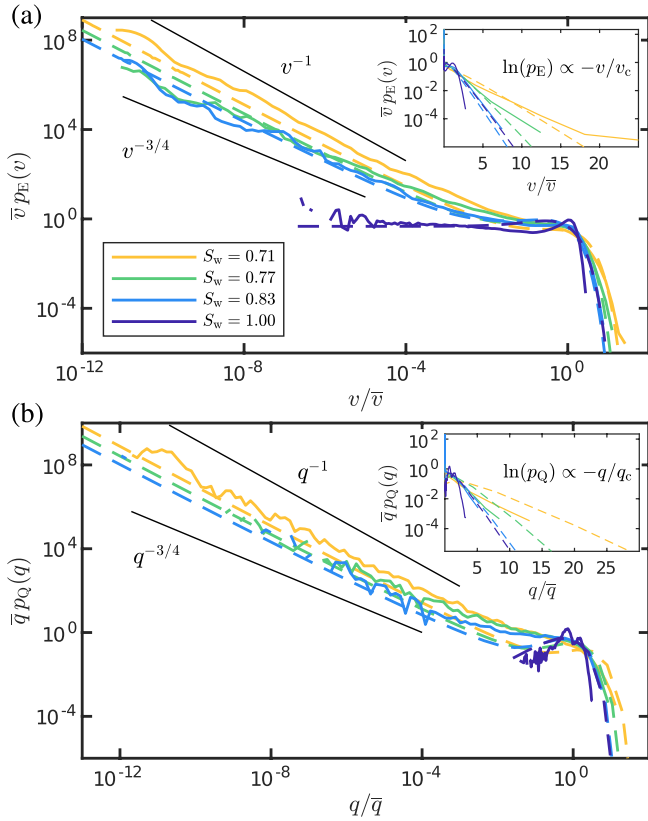


Figure 2. Numerical (continuous lines) and predicted (dashed lines) probability density functions (PDFs) for (a) Eulerian velocities and (b) pore flow rates, normalized by their respective average values \bar{v} and \bar{q} , for $S_w = 1.00, 0.83, 0.77$, and 0.71 . The log–log scale highlights the scaling of low magnitudes; the power law scalings are shown for visual reference. Semi-log insets highlight the exponential behavior at high magnitudes.

3.2. Theoretical Flow Model

To derive a theoretical framework for $p_E(v)$, we first consider the local flow rate through a pore throat, or pore flow rate q . It is computed by integrating flow velocities over the cross section of the pore throat. For all unsaturated conditions, the PDF of pore flow rates over the ensemble of throats $p_Q(q)$ shows a scaling similar to that of $p_E(v)$ for both low and high magnitudes (Figure 2a). However, for $S_w = 1.00$, $p_Q(q)$ increases with q at low values instead of the plateau observed for $p_E(v)$. For $S_w = 1.00$, $p_Q(q)$ is well captured by the flow rate PDF in the backbone p_Q^b , which follows a gamma distribution,

$$p_Q^b(q) = \frac{q e^{-q/q_c}}{q_c^2}, \quad (1)$$

where the saturation-dependent characteristic flow rate q_c controls the exponential high-flow tailing. This is consistent with the random aggregation model of Alim et al. (2017), based on the random splitting and merging of flow throughout the pore network (Coppersmith, 1996).

To model $p_Q(q)$ and $p_E(v)$ for $S_w < 1.00$, we quantify the flow statistics in backbone (p_Q^b) and dead-end (p_Q^d) regions. We first determine the ratio f of the area occupied by dead-end regions to the total area of the pore space (e.g., 0.2601 for $S_w = 0.71$, refer to Supporting Information S1 for the remaining S_w). We express $p_Q(q)$ as

$$p_Q(q) = f p_Q^d(q) + (1 - f) p_Q^b(q). \quad (2)$$

Next, we determine p_Q^d . Simulation data suggest that flow rate magnitudes within dead-end regions decay exponentially with depth $0 \leq z \leq \ell$ (see Supporting Information S1), up to the total depth ℓ of the dead-end region, which extends from the contact with the backbone to the far liquid–gas boundary (see inset in Figure 1d). Such exponential decay is consistent with the fundamental solutions of the Laplace equation for the propagation within the dead-end of the pressure perturbation applied from the boundary with the backbone (Bland, 1965). We expect macroscopic pressure gradients within dead-end regions to obey a Laplace equation resulting from Darcy’s law (Whitaker, 1986). We thus approximate the flow rate decay along the depth as

$$q_d(z|\ell) \approx q_0 e^{-z/a_m} H(\ell - z), \quad (3)$$

where $q_0 = q_d(0|\ell)$ is the flow rate at the contact with the backbone and H is the Heaviside step function. Since this flow rate profile is monotonically decreasing, the associated PDF for a given q_0 and ℓ can be computed as (Aquino & Le Borgne, 2021)

$$p_Q^d(q|\ell, q_0) = \left(\ell \left. \frac{dq_d(z|\ell)}{dz} \right|_{z=z_q(q)} \right)^{-1}, \quad (4)$$

where $z_q(q)$ is the point at which the flow has a given value q , that is, $q_d[z_q(q)|\ell] = q$. Thus, inverting Equation 3 for depth as a function of flow rate, computing $dq_d(z|\ell)/dz$, and substituting, Equation 4 becomes

$$p_Q^d(q|\ell, q_0) = \frac{a_m}{\ell q} H(q_0 - q) H(q - q_0 e^{-\ell/a_m}), \quad (5)$$

for the dead-end flow rate PDF $p_Q^d(\cdot|\ell, q_0)$, given maximum depth ℓ and flow rate $q_0 = q_d(0|\ell)$ at the entrance. Taking q_0 to be distributed according to Equation 1 and averaging over the latter, we can now express the flow rate PDF in dead-ends given ℓ as

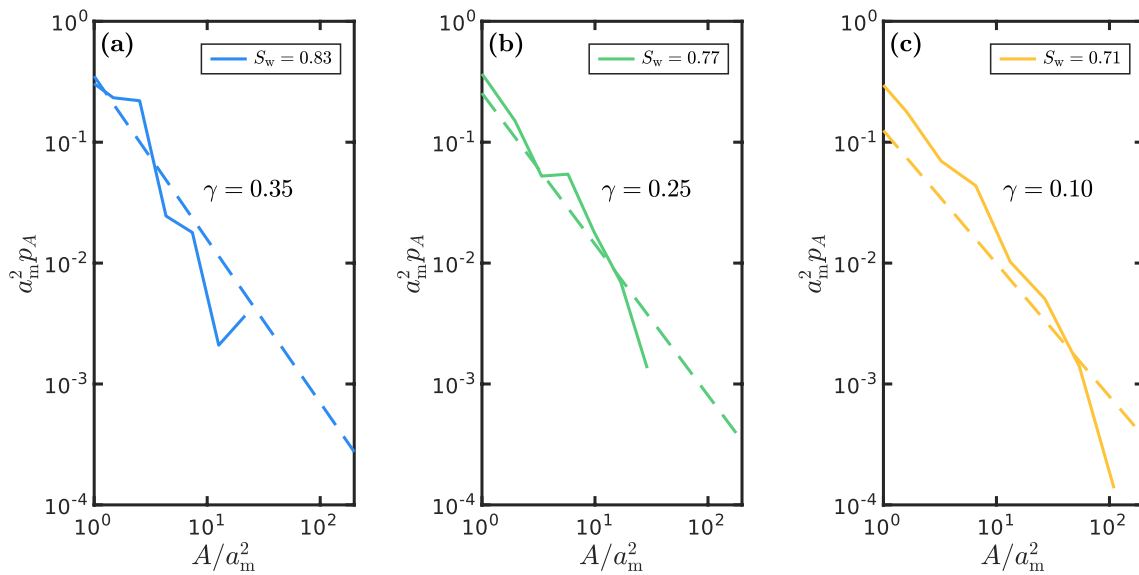


Figure 3. PDF of the dead-end areas p_A for (a) $S_w = 0.83$, (b) $S_w = 0.77$, and (c) $S_w = 0.71$. For all three cases, p_A is well approximated by a Pareto PDF (Equation 9) describing power law decay. Corresponding values of the fitting parameter γ describing a power law decay $\propto A^{-1-\gamma}$, which decreases with decreasing liquid-phase saturation, are also shown. Quantities are non-dimensionalized with respect to the area a_m^2 associated with the average pore-throat aperture.

$$p_Q^d(q|\ell) = \int_0^\infty dq_0 p_Q^d(q|\ell, q_0) p_Q^b(q_0), \quad (6)$$

which after computing the integral leads to

$$p_Q^d(q|\ell) = \frac{a_m}{\ell q_c q} \left[e^{-q/q_c}(q + q_c) - \exp\left(-\frac{e^{\ell/a_m} q}{q_c}\right) (e^{\ell/a_m} q + q_c) \right]. \quad (7)$$

By approximating $\ell \approx \sqrt{A}$, with A the dead-end area, and averaging over areas, we obtain an expression for the PDF of dead-end flow rates,

$$p_Q^d(q) \approx \int_0^\infty dA p_Q^d(q|\sqrt{A}) p_A(A). \quad (8)$$

The PDF p_A of dead-end areas, defined for a given flow field such that $p_A(A) dA$ is the probability of a uniformly randomly chosen dead-end region to have area in an infinitesimal neighborhood dA of A , is shown in Figure 3 for each unsaturated flow field. The area PDFs were determined based on the flow field partitions, as shown in Figure 1 for $S_w = 0.83$ and $S_w = 0.71$. We approximate p_A by a Pareto PDF,

$$p_A(A) = \frac{\gamma}{a_m^2} \left(\frac{A}{a_m^2} \right)^{-1-\gamma} H(A - a_m^2), \quad (9)$$

where the exponent γ decreases with decreasing S_w , indicating broader dead-end area variability. The approximations thus obtained are plotted as dashed lines in Figure 3. We consider the minimum area of a dead-end region to be equal to the area of one pore throat, approximated as a_m^2 .

We can now expand the integrand in Equation 8 using Equation 9, obtaining

$$p_Q^d(q) \approx \int_0^\infty dA \frac{a_m}{q_c \sqrt{A}} e^{-q/q_c} p_A(A). \quad (10)$$

Computing this integral, and combining it with the expression for $p_Q^b(q)$ (Equation 1) in Equation 2, we deduce an expression for $p_Q(q)$. For $q \ll q_c$, the latter is controlled by the dead-end contribution as long as $f \neq 0$,

corresponding to $S_w < 1.00$. Notice also that the nested exponential in Equation 7 varies rapidly from zero to unity around $q = q_c e^{-\ell/a_m}$, so that it is well approximated by a cutoff for $A \approx \ell^2 > [a_m \ln(q_c/q)]^2$. This leads to

$$p_Q^d(q) \approx \int_0^\infty dA \frac{a_m}{q_c \sqrt{A}} \left[1 - H \left(\left[a_m \ln \left(\frac{q_c}{q} \right) \right]^2 - A \right) \right] p_A(A), \quad (11)$$

$$\approx \frac{2\gamma}{q(1+2\gamma)} \left[\ln \left(\frac{q_c}{q} \right) \right]^{-1-2\gamma}, \quad q \ll q_c,$$

which, combined with Equations 1 and 2, leads to

$$p_Q(q) \approx \frac{2\gamma f}{q(1+2\gamma)} \left[\ln \left(\frac{q_c}{q} \right) \right]^{-1-2\gamma}. \quad (12)$$

Thus, our model predicts that for $S_w < 1.00$, $p_Q(q)$ scales for low flow rates as a power law, q^{-1} , corrected by a logarithmic factor, raised to a power controlled by $p_A(A)$ through the exponent γ . In the particular case $f = 0$, that is, $S_w = 1.00$, Taylor expansion of p_Q^b (Equation 1) for low q leads to $p_Q(q) \approx q/q_c^2$, linear in q . Proceeding similarly for $q \gtrsim q_c$, for which we must consider contributions from both $p_Q^b(q)$ and $p_Q^d(q)$, we obtain the exponential decay

$$p_Q(q) \approx \left[\frac{2\gamma f}{1+2\gamma} + (1-f) \frac{q}{q_c} \right] \frac{e^{-q/q_c}}{q_c}. \quad (13)$$

We now turn our attention to $p_E(v)$. It results from the combined effect of $p_Q(q)$ and the intra-throat variability arising from the local velocity profile within each throat. Thus, these two PDFs are related by

$$p_E(v) = \int_0^\infty dq p_Q(q) p_E(v|q), \quad (14)$$

where $p_E(\cdot|q)$ is the PDF of velocities associated with a pore throat characterized by q . Since pore-throat widths are comparable in size to the channel thickness h , we consider the impact of this third dimension on the intrapore, depth-averaged 2D velocity profile. The latter differs from the parabolic profile expected in a purely 2D scenario (see Supporting Information S1 for plot of velocity profiles across the system). By approximating the pore throat as a cuboid channel of width a_m and thickness h , we express the velocity profile for Stokes flow over the channel thickness h as a series in the form (Bruus, 2008):

$$v_x(y, z) = \frac{4h^2 \Delta p}{\pi^3 \mu L} \sum_{n, \text{odd}} \frac{1}{n^3} \left[1 - \frac{\cosh \left(n\pi \frac{y}{h} \right)}{\cosh \left(n\pi \frac{a_m}{2h} \right)} \right] \sin \left(n\pi \frac{z}{h} \right), \quad (15)$$

where μ is the viscosity of the liquid (wetting) phase, Δp is the pressure difference across the cuboid channel of length L , and the sum extends over odd values of n as indicated. Here, we have set a local coordinate system at each pore throat, with x representing the local mean flow direction, the throat width running parallel to y , and z running along the channel thickness. Averaging this function over z values between 0 and h , we obtain

$$\langle v_x(y, z) \rangle_z = \frac{8h^2 \Delta p}{\pi^4 \mu L} \sum_{n, \text{odd}} \frac{1}{n^4} \left[1 - \frac{\cosh \left(n\pi \frac{y}{h} \right)}{\cosh \left(n\pi \frac{a_m}{2h} \right)} \right], \quad (16)$$

where $\langle \cdot \rangle$ denotes the mean value. Given the low variability of pore-throat sizes across the medium, we approximate throat widths by their average value a_m . For the dimensions of our porous medium (thickness h and average throat width a_m), this series is governed by its first term, reducing the expression to

$$\langle v_x(y, z) \rangle_z \approx \frac{h^2 \Delta p}{2\pi^4 \mu L} \left[1 - \frac{\cosh \left(2\pi \frac{y}{h} \right)}{\cosh \left(\pi \frac{a_m}{h} \right)} \right]. \quad (17)$$

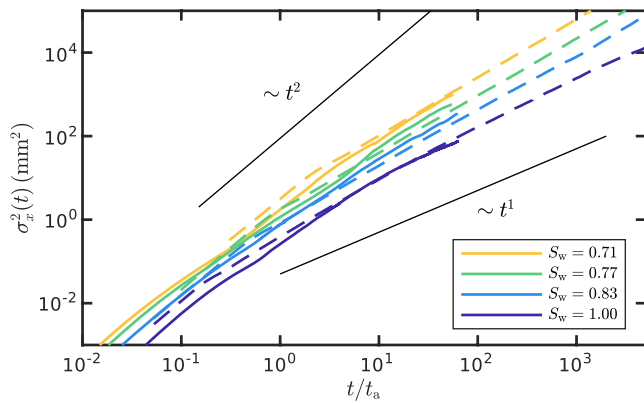


Figure 4. Advective dispersion σ_x^2 in time for $S_w = 1.00, 0.83, 0.77,$ and 0.71 . Time is normalized by the advective time $t_a = \lambda/\bar{v}$ over the mean pore size λ . The plot compares σ_x^2 from the particle tracking analysis (continuous lines) with σ_x^2 from a continuous time random walk (CTRW) approach computed using the predicted velocity PDF $p_E(v)$ (dashed lines). Scalings for a ballistic ($\sigma_x^2 \sim t^2$) and a Fickian ($\sigma_x^2 \sim t^1$) regime are also displayed for reference.

The Eulerian velocity PDF associated with the velocity profile across a pore throat with local flow rate q is then (see Supporting Information S1 for further details)

$$p_E(v|q) = \frac{2h}{\pi a_m v_{\max}(q)} \frac{(C-1)H[v_{\max}(q)-v]}{\sqrt{[C-(C-1)v/v_{\max}(q)]^2-1}}, \quad (18)$$

where $C = \cosh[\pi a_m/(2h)]$, and $v_{\max}(q) = \alpha q/(h a_m)$ is the maximum velocity within the pore throat, with

$$\alpha = 2 \left(1 + \coth\left(\frac{\pi a_m}{4h}\right) \left[\coth\left(\frac{\pi a_m}{4h}\right) - \frac{4h}{\pi a_m} \right] \right)^{-1}. \quad (19)$$

For $S_w = 1.00$, the integral in Equation 14 can then be approximated for $v \ll v_c$ and $v \gtrsim v_c = q_c/(a_m h)$, respectively, by using Equation 1, as

$$p_E(v) \approx \frac{2h}{\pi a_m \alpha v_c} \tanh\left(\frac{\pi a_m}{4h}\right), \quad (20a)$$

$$p_E(v) \approx \frac{2h}{\alpha a_m v_c} \sinh\left(\frac{\pi a_m}{4h}\right) \sqrt{\frac{v}{\pi \alpha v_c}} e^{-\frac{v}{\alpha v_c}}. \quad (20b)$$

Equation 20a describes a low-velocity plateau, while Equation 20b encodes exponential tailing at large velocities.

For $S_w < 1.00$, the previous derivation holds for the backbone component. Similar to $p_Q(q)$, $p_E(v)$ for $v \ll v_c$ is dominated by the dead-end regions, while for $v \gtrsim v_c$ the contribution of both backbone and dead-ends matters. The low-velocity behavior is controlled by low flow rates. For small q , $p_E(v|q)$ becomes arbitrarily narrow, because the maximum velocity is linear in q , see Equation 18. Accordingly, $p_E(v)$ is well approximated for low v by setting $p_E(v|q) \approx \delta[v - q/(h a_m)]$ in Equation 14, where $\delta(\cdot)$ is the Dirac delta, and by using Equation 12 for $p_Q(q)$. We obtain, for $v \ll v_c$,

$$p_E(v) \approx \frac{2\gamma f}{v(1+2\gamma)} \left[\ln\left(\frac{v_c}{v}\right) \right]^{-1-2\gamma}. \quad (21)$$

Analogously, for $v \gtrsim v_c$, $p_E(v)$ can be computed using Equation 13 for $p_Q(q)$, and Taylor expanding Equation 18 for $v \approx v_{\max}(q)$, which leads to

$$p_E(v) \approx \left[\frac{2\gamma f}{1+2\gamma} \sqrt{\frac{\alpha v_c}{v}} + (1-f) \sqrt{\frac{v}{\alpha v_c}} \right] \frac{C_* e^{-\frac{v}{\alpha v_c}}}{\alpha v_c}, \quad (22)$$

where $C_* = 2h \sinh(\pi a_m/4h)/(\sqrt{\pi a_m})$. Note that for large h values compared to a_m , Equations 20a–22 reduce to expressions that correspond to those obtained under the assumption of a Poiseuille velocity profile (fully 2D case; see Supporting Information S1 for a complete mathematical deduction).

Figure 2 shows the predictions (dashed lines) for both $p_Q(q)$ and $p_E(v)$. The model successfully captures the different regimes and scaling variation for the various S_w . The low-velocity plateau for $S_w = 1.00$ is also captured. The results shown here correspond to numerical computation of the full theoretical PDFs according to Equations 1, 2, 8, and 14. Further details on the regime scalings and parameter values can be found in the Supporting Information S1.

4. Prediction of Advective Transport

Using the results of the particle tracking simulations (see Section 2.2), we compute (advective) dispersion $\sigma_x^2(t)$, as a function of time t , as the variance of longitudinal particle positions. Lower saturation induces larger particle dispersion due to the increased velocity heterogeneity, as discussed above. At early times, a ballistic regime, $\sigma_x^2 \sim t^2$ is observed in Figure 4 for all S_w , which then transitions to an asymptotic superdiffusive regime. The crossover time between the ballistic and asymptotic regimes is also larger for smaller S_w , that is, the Lagrangian

correlation length ζ_x of velocities along the mean flow direction increases with decreasing saturation (refer to Supporting Information S1 for correlation plots).

To develop a transport modeling framework that links the dispersion dynamics to hydrodynamics, we employ a CTRW approach (Berkowitz et al., 2006; Cortis & Berkowitz, 2004; Dentz et al., 2016). The CTRW framework used here models transport in terms of Lagrangian particles taking fixed spatial steps of length ζ_x along the mean flow direction (*s*-Lagrangian sampling). Particle velocities remain constant over a step and are assumed to fully decorrelate between steps. They are sampled independently in each step from the *s*-Lagrangian velocity distribution, which is given by the flux-weighted $p_E(v)$, $p_s(v) = v p_E(v) / \bar{v}$ (Dentz et al., 2016). This approach captures the intermittent nature of the *t*-Lagrangian velocity signal through the distributed waiting times to cross the fixed distance ζ_x .

To assess the applicability of our theoretical model to predict advective transport, we employ $p_s(v)$ defined from the predicted $p_E(v)$ (dashed lines in Figure 2a) in the CTRW description. Figure 4 shows σ_x^2 computed from the resulting CTRW for each S_w (dashed lines), together with σ_x^2 computed from the particle tracking simulations. Dispersion is well predicted over both the ballistic and superdiffusive regimes, and so the impact of S_w on the temporal scaling. A slight overestimation of early-time dispersion is visible for $S_w = 1.00$, which might be explained by the assumption of full velocity decorrelation beyond ζ_x . Late-time dispersion is well captured in all cases, exhibiting more pronounced superdiffusive behavior for $S_w < 1.00$. Overall, these results support the suitability of both our theoretical description of velocity statistics and the CTRW to predict advective transport in unsaturated porous media, representing a major step toward predicting solute transport in such systems from the sole knowledge of the medium's geometry.

The CTRW model presented here provides a theoretical framework to quantify the relationship between dispersive scalings and velocity variability. In particular, the late-time scaling is controlled by the low-velocity behavior of $p_E(v)$. If $p_E(v)$ exhibits power law decay near $v = 0$, $p_E(v) \sim v^{-\theta}$ with $0 < \theta < 1$, late-time dispersion scales like $\sigma_x^2 \sim t^{1+\theta}$ (Dentz et al., 2016), between the Fickian and ballistic limits $\sigma_x^2 \sim t$ and $\sigma_x^2 \sim t^2$. The scalings found here for saturated and unsaturated conditions correspond to two contrasting edge-cases. Under saturated conditions, $\theta = 0$ (Equation 20a), which leads to logarithmically enhanced Fickian dispersion (Dentz et al., 2016). Note that pure power law decay characterized by $\theta \geq 1$ is not integrable near $v = 0$. In this sense, unsaturated conditions are characterized by maximal variability of low velocities, described by logarithmic corrections to power law decay with $\theta = 1$ (Equation 21). This leads to logarithmically inhibited ballistic dispersion. In light of these considerations, along with the fact that the unsaturated $p_E(v)$ is broader than for the saturated case (Figure 2), the apparent power law scalings in Figure 4 vary slowly with time, as logarithmic corrections and the effect of progressively lower velocities come into play. A rigorous derivation of asymptotic dispersion scalings is beyond the scope of this work and will be presented elsewhere.

5. Conclusions and Outlook

Here, we have presented a new theoretical framework for the prediction of pore-scale flow PDFs and advective transport capturing the impact of liquid-phase saturation. Results reveal that the introduction of an immiscible gas phase leads to a shift in the scaling of the velocity PDFs that induces a sharp transition to strongly anomalous transport. Under saturated conditions, dispersion is quasi-Fickian. In contrast, even under slightly unsaturated conditions, dispersion becomes quasi-ballistic. In practice, this superdiffusive dispersion behavior is sustained until low-velocity cutoffs introduced by additional processes, such as diffusion, become relevant. The long-term residence time of a particle in a dead-end region is eventually controlled by molecular diffusion, effectively cutting off extreme slow velocities (de Gennes, 1983). While in the presence of diffusion the transport is thus always asymptotically Fickian at sufficiently late times, the dispersive scalings related to the velocity variability remain relevant over significant time scales. Our CTRW formulation also opens the door to the quantification of nontrivial scalings of dispersion (Aquino & Le Borgne, 2021; Bijeljic & Blunt, 2006).

The theoretical formulation developed here successfully predicts flow and velocity PDFs based only on a small set of parameters, which reflect characteristics of the porous medium (average pore-throat width a_m and thickness h), the relative occupancy of backbone and dead-ends in the system (power law tailing exponent γ and ratio of dead-end area to total pore-space area f), and flow properties (correlation length of longitudinal velocities ζ_x and tortuosity χ , along with the characteristic flow rate q_c , used to determine the characteristic velocity $v_c = q_c / (h a_m)$).

While the values of these parameters depend on properties such as porosity and liquid-phase saturation, we expect the uncovered transition in the velocity PDF and its impact on transport scaling properties to be robust.

We expect the power law dead-end area distribution to hold for (quasi-)2D systems, independently of the detailed pore geometry. In particular, it holds for fully 2D systems and so does the spatial distribution of pore flow rates in dead-end regions (Equation 3), providing good predictions for $h/a_m \gg 1$. In addition, we also expect it to persist in 3D systems, as is known to happen for both wetting- and nonwetting-phase cluster size distributions (Iglauer et al., 2010, 2012; Scheffer et al., 2021). These authors also report this behavior for wetting-phase saturation degrees lower than 0.71, which we could not achieve in the present study, as they would approach the percolation threshold for the experimental medium. However, following previous works that report a decrease in dispersivity once the system is desaturated below the so-called critical saturation (Raouf & Hassanizadeh, 2013), we hypothesize a decrease in the broadness of the velocity distribution through an increase in the dead-end area-PDF exponent γ for saturation degrees below that critical saturation. In addition, although the present study considers a high porosity (0.71), the distribution of nonwetting-phase cluster sizes still exhibits power-law behavior for porosity values as low as 0.11 (Iglauer et al., 2010, 2012; Scheffer et al., 2021). The effect of broader pore size variability (de Anna et al., 2017) under unsaturated conditions remains an important open question. Note, however, that even if a different functional dependency were observed for the dead-end area PDF, our new theoretical framework provides the means to quantify its impact on flow velocity distributions and transport. Furthermore, the upscaling of flow and transport presented here is a first step toward theoretical assessment of mixing and chemical reactions in unsaturated porous media, which are essential processes for the analysis and optimization of environmental and industrial systems.

Data Availability Statement

The raw experimental images for all four saturation degrees, employed in the numerical simulations, are available under open access in Jiménez-Martínez et al. (2017) (<https://doi.org/10.1002/2016WR019849>).

Acknowledgments

A.V.-P. and J.J.-M. gratefully acknowledge the financial support from the Swiss National Science Foundation (SNF, grant nr. 200021 178986). T.A. is supported by a Marie Skłodowska Curie Individual Fellowship, funded by the European Union's Horizon 2020 research and innovation program under the project *ChemicalWalks* 838426. Y.M. and T.L.B. acknowledge funding from ERC project *ReactiveFronts* 648377. Open access funding provided by ETH-Bereich Forschungsanstalten.

References

- Alim, K., Parsa, S., Weitz, D. A., & Brenner, M. P. (2017). Local pore size correlations determine flow distributions in porous media. *Physical Review Letters*, 119(14), 144501. <https://doi.org/10.1103/PhysRevLett.119.144501>
- Andrade, J. S., Jr., Almeida, M. P., Mendes Filho, J., Havlin, S., Suki, B., & Stanley, H. E. (1997). Fluid flow through porous media: The role of stagnant zones. *Physical Review Letters*, 79(20), 3901–3904. <https://doi.org/10.1103/PhysRevLett.79.3901>
- Aquino, T., & Le Borgne, T. (2021). The diffusing-velocity random walk: A spatial-Markov formulation of heterogeneous advection and diffusion. *Journal of Fluid Mechanics*, 910, A12. <https://doi.org/10.1017/jfm.2020.957>
- Aziz, R., Joekar-Niasar, V., & Martínez-Ferrer, P. (2018). Pore-scale insights into transport and mixing in steady-state two-phase flow in porous media. *International Journal of Multiphase Flow*, 109, 51–62. <https://doi.org/10.1016/j.ijmultiphaseflow.2018.07.006>
- Barbier, E. (2002). Geothermal energy technology and current status: An overview. *Renewable and Sustainable Energy Reviews*, 6(1–2), 3–65. [https://doi.org/10.1016/S1364-0321\(02\)00002-3](https://doi.org/10.1016/S1364-0321(02)00002-3)
- Berkowitz, B., Cortis, A., Dentz, M., & Scher, H. (2006). Modeling non-Fickian transport in geological formations as a continuous time random walk. *Reviews of Geophysics*, 44, RG2003. <https://doi.org/10.1029/2005RG000178>
- Bijeljic, B., & Blunt, M. J. (2006). Pore-scale modeling and continuous time random walk analysis of dispersion in porous media. *Water Resources Research*, 42, W01202. <https://doi.org/10.1029/2005WR004578>
- Bijeljic, B., Rubin, S., Scher, H., & Berkowitz, B. (2011). Non-Fickian transport in porous media with bimodal structural heterogeneity. *Journal of Contaminant Hydrology*, 120–121, 213–221. <https://doi.org/10.1016/j.jconhyd.2010.05.007>
- Birkholzer, J., & Tsang, C.-f. (1997). Solute channeling in unsaturated heterogeneous porous media. *Water Resources Research*, 33(10), 2221–2238. <https://doi.org/10.1029/97WR01209>
- Bland, D. R. (1965). *Solutions of Laplace's equation*. Plymouth: Routledge.
- Bouwer, H. (2002). Artificial recharge of groundwater: Hydrogeology and engineering. *Hydrogeology Journal*, 10(1), 121–142. <https://doi.org/10.1007/s10040-001-0182-4>
- Bromly, M., & Hinz, C. (2004). Non-Fickian transport in homogeneous unsaturated repacked sand. *Water Resources Research*, 40, W07402. <https://doi.org/10.1029/2003WR002579>
- Bruus, H. (2008). *Theoretical microfluidics—Oxford master series in condenser matter physics*. Oxford University Press.
- Coppersmith, D. (1996). *Advances in cryptology—Eurocrypt '96, Lecture notes in computer science* (Vol. 1070). Berlin: Springer.
- Cortis, A., & Berkowitz, B. (2004). Anomalous transport in “classical” soil and sand columns. *Soil Science Society of America Journal*, 68(5), 1539–1548. <https://doi.org/10.2136/sssaj2004.1539>
- Datta, S. S., Chiang, H., Ramakrishnan, T. S., & Weitz, D. A. (2013). Spatial fluctuations of fluid velocities in flow through a three-dimensional porous medium. *Physical Review Letters*, 111(6), 064501. <https://doi.org/10.1103/PhysRevLett.111.064501>
- de Anna, P., Le Borgne, T., Dentz, M., Tartakovsky, A. M., Bolster, D., & Davy, P. (2013). Flow intermittency, dispersion, and correlated continuous time random walks in porous media. *Physical Review Letters*, 110(18), 184502. <https://doi.org/10.1103/PhysRevLett.110.184502>
- de Anna, P., Quaipe, B., Biros, G., & Juanes, R. (2017). Prediction of the low-velocity distribution from the pore structure in simple porous media. *Physical Review Fluids*, 2(12), 124103. <https://doi.org/10.1103/PhysRevFluids.2.124103>

- de Gennes, P. G. (1983). Hydrodynamic dispersion in unsaturated porous media. *Journal of Fluid Mechanics*, *136*, 189–200. <https://doi.org/10.1017/s0022112083002116>
- Dentz, M., Kang, P. K., Comolli, A., Le Borgne, T., & Lester, D. R. (2016). Continuous time random walks for the evolution of Lagrangian velocities. *Physical Review Fluids*, *1*(7), 074004. <https://doi.org/10.1103/PhysRevFluids.1.074004>
- Ferrari, A., Jiménez-Martínez, J., Le Borgne, T., Meheust, Y., & Lunati, I. (2015). Challenges in modeling unstable two-phase flow experiments in porous micromodels. *Water Resources Research*, *51*, 1381–1400. <https://doi.org/10.1002/2014WR016384>
- Haga, D., Niibori, Y., & Chida, T. (1999). Hydrodynamic dispersion and mass transfer in unsaturated flow. *Water Resources Research*, *35*(4), 1065–1077. <https://doi.org/10.1029/1998WR900111>
- Holzner, M., Morales, V. L., Willmann, M., & Dentz, M. (2015). Intermittent Lagrangian velocities and accelerations in three-dimensional porous medium flow. *Physical Review E*, *92*(1), 013015. <https://doi.org/10.1103/PhysRevE.92.013015>
- Iglauer, S., Favretto, S., Spinelli, G., Schena, G., & Blunt, M. J. (2010). X-ray tomography measurements of power-law cluster size distributions for the nonwetting phase in sandstones. *Physical Review E*, *82*(5), 056315. <https://doi.org/10.1103/PhysRevE.82.056315>
- Iglauer, S., Fernø, M. A., Shearing, P., & Blunt, M. J. (2012). Comparison of residual oil cluster size distribution, morphology and saturation in oil-wet and water-wet sandstone. *Journal of Colloid and Interface Science*, *375*(1), 187–192. <https://doi.org/10.1016/j.jcis.2012.02.025>
- Jiménez-Martínez, J., de Anna, P., Tabuteau, H., Turuban, R., Borgne, T. L., & Méheust, Y. (2015). Pore-scale mechanisms for the enhancement of mixing in unsaturated porous media and implications for chemical reactions. *Geophysical Research Letters*, *42*, 5316–5324. <https://doi.org/10.1002/2015GL064513>
- Jiménez-Martínez, J., Le Borgne, T., Tabuteau, H., & Méheust, Y. (2017). Impact of saturation on dispersion and mixing in porous media: Photobleaching pulse injection experiments and shear-enhanced mixing model. *Water Resources Research*, *53*, 1457–1472. <https://doi.org/10.1002/2016WR019849>
- Kang, P. K., de Anna, P., Nunes, J. P., Bijeljic, B., Blunt, M. J., & Juanes, R. (2014). Pore-scale intermittent velocity structure underpinning anomalous transport through 3-D porous media. *Geophysical Research Letters*, *41*, 6184–6190. <https://doi.org/10.1002/2014GL061475>
- Kazemifar, F., Blois, G., Kyritsis, D. C., & Christensen, K. T. (2016). Quantifying the flow dynamics of supercritical CO₂-water displacement in a 2D porous micromodel using fluorescent microscopy and microscopic PIV. *Advances in Water Resources*, *95*, 352–368. <https://doi.org/10.1016/j.advwatres.2015.05.011>
- Lahav, O., Kochva, M., & Tarchitzky, J. (2010). Potential drawbacks associated with agricultural irrigation with treated wastewaters from desalinated water origin and possible remedies. *Water Science and Technology*, *61*(10), 2451–2460. <https://doi.org/10.2166/wst.2010.157>
- Le Borgne, T., Bolster, D., Dentz, M., de Anna, P., & Tartakovsky, A. (2011). Effective pore-scale dispersion upscaling with a correlated continuous time random walk approach. *Water Resources Research*, *47*, W12538. <https://doi.org/10.1029/2011WR010457>
- Morales, V. L., Dentz, M., Willmann, M., & Holzner, M. (2017). Stochastic dynamics of intermittent pore-scale particle motion in three-dimensional porous media: Experiments and theory. *Geophysical Research Letters*, *44*, 9361–9371. <https://doi.org/10.1002/2017GL074326>
- Moroni, M., Kleinfelder, N., & Cushman, J. H. (2007). Analysis of dispersion in porous media via matched-index particle tracking velocimetry experiments. *Advances in Water Resources*, *30*(1), 1–15. <https://doi.org/10.1016/j.advwatres.2006.02.005>
- Nützmann, G., Maciejewski, S., & Joswig, K. (2002). Estimation of water saturation dependence of dispersion in unsaturated porous media: Experiments and modelling analysis. *Advances in Water Resources*, *25*, 565–576. [https://doi.org/10.1016/S0309-1708\(02\)00018-0](https://doi.org/10.1016/S0309-1708(02)00018-0)
- Padilla, I. Y., Yah, T.-C. J., & Conklin, M. H. (1999). The effect of water content on solute transport in unsaturated porous media. *Water Resources Research*, *35*(11), 3303–3313. <https://doi.org/10.1029/1999WR900171>
- Panfilov, M. (2010). Underground storage of hydrogen: In situ self-organisation and methane generation. *Transport in Porous Media*, *85*(3), 841–865. <https://doi.org/10.1007/s11242-010-9595-7>
- Raoof, A., & Hassanizadeh, S. M. (2013). Saturation-dependent solute dispersivity in porous media: Pore-scale processes. *Water Resources Research*, *49*, 1943–1951. <https://doi.org/10.1002/wrcr.20152>
- Scheffer, K., Méheust, Y., Carvalho, M. S., Mauricio, M. H., & Paciornik, S. (2021). Enhancement of oil recovery by emulsion injection: A pore scale analysis from X-ray micro-tomography measurements. *Journal of Petroleum Science and Engineering*, *198*, 108134. <https://doi.org/10.1016/j.petrol.2020.108134>
- Sebilo, M., Mayer, B., Nicolardot, B., Pinay, G., & Mariotti, A. (2013). Long-term fate of nitrate fertilizer in agricultural soils. *Proceedings of the National Academy of Sciences of the United States of America*, *110*(45), 18185–18189. <https://doi.org/10.1073/pnas.1305372110>
- Stoop, N., Waisbord, N., Kantsler, V., Heinonen, V., Guasto, J. S., & Dunkel, J. (2019). Disorder-induced topological transition in porous media flow networks. *Journal of Non-Newtonian Fluid Mechanics*, *268*, 66–74. <https://doi.org/10.1016/j.jnnfm.2019.05.002>
- Tallakstad, K. T., Løvoll, G., Knudsen, H. A., Ramstad, T., Flekkøy, E. G., & Måløy, K. J. (2009). Steady-state, simultaneous two-phase flow in porous media: An experimental study. *Physical Review E*, *80*(3), 036308. <https://doi.org/10.1103/PhysRevE.80.036308>
- Tang, J., Smit, M., Vincent-Bonnieu, S., & Rossen, W. R. (2019). New Capillary Number definition for micromodels: The impact of pore microstructure. *Water Resources Research*, *55*, 1167–1178. <https://doi.org/10.1029/2018WR023429>
- Vanderborght, J., & Vereecken, H. (2007). Review of dispersivities for transport modeling in soils. *Vadose Zone Journal*, *6*(1), 29–52. <https://doi.org/10.2136/vzj2006.0096>
- Whitaker, S. (1986). Flow in porous media I: A theoretical derivation of Darcy's law. *Transport in Porous Media*, *1*(1), 3–25. <https://doi.org/10.1007/BF01036523>
- Wildenschild, D., & Jensen, K. H. (1999). Laboratory investigations of effective flow behavior in unsaturated heterogeneous sands. *Water Resources Research*, *35*(1), 17–27. <https://doi.org/10.1029/98WR01958>
- Winograd, I. (1981). Radioactive waste disposal in thick unsaturated zones. *Science*, *212*(4502), 1457–1914. <https://doi.org/10.1126/science.212.4502.1457>